Journal of Quantitative Spectroscopy & Radiative Transfer 113 (2012) 2512–2520

Contents lists available at SciVerse ScienceDirect

Journal of Quantitative Spectroscopy & Radiative Transfer

journal homepage: www.elsevier.com/locate/jqsrt

Evanescent wave optical trapping and transport of micro- and nanoparticles on tapered optical fibers

S.E. Skelton [a], M. Sergides [a], R. Patel [a], E. Karczewska [a], O.M. Maragó [b], P.H. Jones [a,*]

[a] Department of Physics and Astronomy, University College London, Gower Street, London WC1E 6BT, UK
[b] CNR-IPCF, Istituto per i Processi Chimico-Fisici, Viale F. Stagno D'Alcontres 37, I-98158 Messina, Italy

ARTICLE INFO

Article history:
Received 16 January 2012
Received in revised form
1 June 2012
Accepted 4 June 2012
Available online 15 June 2012

Keywords:
Optical trapping
Optical binding
Optical fiber
Plasmon resonance

ABSTRACT

We investigate the manipulation of microscopic and nanoscopic particles using the evanescent optical field surrounding an optical fiber that is tapered to a micron-scale diameter, and propose that this scheme could be used to discriminate between, and thereby sort, metallic nanoparticles. First we show experimentally the concept of the transport of micron-sized spheres along a tapered fiber and measure the particle velocity. Having demonstrated the principle we then consider theoretically the application to the optical trapping and guiding of metallic nanoparticles, where the presence of a plasmon resonance is used to enhance optical forces. We show that the dynamics of the nanoparticles trapped by the evanescent field can be controlled by the state of polarization of the fiber mode, and by using more than one wavelength differently detuned from the nanoparticle plasmon resonance. Such a scheme could potentially be used for selectively trapping and transporting nano- or microscopic material from a polydisperse suspension.

1. Introduction

It has long been known that a laser beam can exert significant optical forces on microscopic particles. Most commonly these forces are utilized in an optical tweezers [1], where a single laser beam is brought to a diffraction-limited spot by a microscope objective lens, capable of producing stable three-dimensional trapping for micron and sub-micron-sized particles. This realization of optical trapping has been applied to a variety of micro- and nanoscale materials including viruses [2], aerosols [3], microbubbles [4], semiconductor nanowires [5], carbon nanotubes [6] and graphene flakes [7]. Similarly, a microparticle exposed to an evanescent optical field experiences a radiative force, as was first demonstrated by the driving of water-suspended particles above the surface of a prism by a single laser beam, weakly focused and undergoing total internal reflection on the prism-to-water interface from below [8]. Later experiments used two counter-propagating laser beams which lead to stable trapping [9,10] and the formation of a variety of self-assembled particle structures dependent on the polarization state of the laser beams [11] or the number of bound particles [12], and enhanced the optical forces by enclosing the experiment in a resonant optical cavity [13].

An alternative scheme for generating an evanescent optical field suitable for trapping is to use an optical fiber that is tapered to a diameter of around 1 μm or smaller. In such ultra-thin fibers a significant fraction of the optical power is contained in an evanescent field around the fiber core which penetrates an appreciable distance into the surrounding medium [14], and such evanescent field fiber traps have been used for trapping [15] and probing [16] laser-cooled atoms in addition to manipulations of microparticles [17]. Similar evanescent wave trapping and propulsion has also been achieved using

* Corresponding author.
E-mail address: philip.jones@ucl.ac.uk (P.H. Jones).

0022-4073/$ - see front matter © 2012 Elsevier Ltd. All rights reserved.
http://dx.doi.org/10.1016/j.jqsrt.2012.06.005

waveguides with a rectangular geometry for both solid [18,19] and hollow particles [20].

In this work we demonstrate fabrication of tapered optical fibers using a simple and low-cost 'heat-and-pull' technique, and show that the biconical tapers produced in this way are suitable for evanescent-wave trapping and propulsion of microscopic spherical particles. Having experimentally demonstrated the principle of operation we then make calculations of the optical trapping and scattering forces on metallic nanoparticles, showing that such forces are enhanced for a trapping wavelength in the vicinity of the nanoparticle's plasmon resonance, and describe a scheme for controlling the nanoparticle trajectory along the taper using bichromatic laser fields and control of the fiber mode polarizations. We suggest that the sensitivity of the nanoparticle dynamics to the polarization and wavelength of the laser fields through the plasmon resonance could make such tapered fibers an effective tool for sorting and separating nanoparticles according to property-dependent criteria.

2. Experiment

2.1. Fabrication of tapered optical fibers

Our tapered optical fibers are produced using a 'heat-and-pull' method similar to that described in [21]. A length of standard single-mode optical fiber (SM-980-125-5.6 from Thorlabs Inc. NJ) has a short region of the protective polymer buffer jacket stripped away and is mounted on a pair of motorized translation stages. The heat source is a hand-held butane gas torch which, unlike the method described in [21,22], is kept static during the pulling process, limiting the length of the tapered region achievable. The fiber is tapered by driving the motorized stages apart a distance of 20–30 mm at speeds of between 0.5 and 1.0 mm s^{-1}. After the tapering process is complete the flame is removed and the tapered fiber mounted on a custom-made microscope slide containing a 300 μm deep slot. A few tens of microliters of solution containing 2 μm diameter polystyrene microspheres suspended in deionized water (with 10% by volume Triton-X-100 to prevent particles sticking to the fiber) is added and sealed beneath a cover slip. Each end of the tapered fiber is cleaved and inserted into a fiber-to-fiber splice unit to couple in laser light. The slide-mounted tapered fiber is then viewed in an inverted microsope (Zeiss Axiovert 200).

2.2. Evanescent wave trapping and propulsion of microparticles

The laser source for these experiment is a single-mode Nd:YAG laser (wavelength $\lambda = 1064$ nm) with a maximum output power of 3 W. The output beam is coupled into a length of the same type of optical fiber that is used for making the fiber tapers using a NA=0.15 collimating lens. These fibers are then connected to the tapered fiber by means of the fiber-to-fiber splice. A diagram of the optical set-up is shown in Fig. 1.

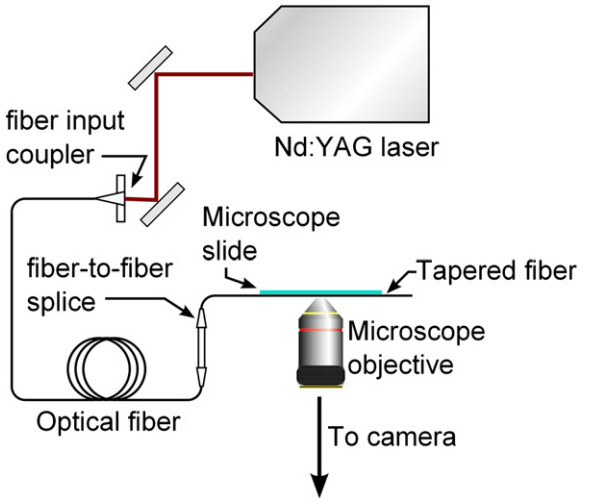

Fig. 1. Diagram of optical set-up. Light from a Nd:YAG laser is coupled into a conventional optical fiber which is spliced to a short length of fiber, the central part of which has been drawn into a biconical taper by the pulling process. The tapered fiber is fixed to a slotted microscope slide and viewed in an inverted microscope.

The waist of the tapered fibers produced by this method is typically around 1 μm. When a single mode propagates unidirectionally in the fiber, microparticles are observed to be trapped against the fiber by the optical gradient force of the evanescent field, and propelled along it by the scattering force in the same direction as the mode propagates. The motion of the particle along the tapered optical fiber is tracked by video microscopy [23], from which we extract the trajectory of the propelled particle and measure its speed along the fiber.

A sequence of images is shown in Fig. 2(a)–(c) that shows a single 2 μm diameter polystyrene sphere pushed along the tapered region of the fiber by radiation pressure. An example of the particle trajectories extracted from a video recording is shown in Fig. 2(d), where the tracks of two particles which are pushed along the fiber are plotted. From a linear fit to the particle track we measure the speed to be $v = (6.98 \pm 0.05)$ μm s^{-1}.

3. Theory

3.1. Distribution of electric field

The electric field distribution in the region of the tapered fiber waist is found by solving the wave equation for the cylindrical boundary conditions of the tapered fiber. A numerical solution of the fiber eigenvalue equation [24] yields the transverse component of the mode wavevector inside the glass fiber, h, which also satisfies

$$h^2 + \beta^2 = n_1^2 k_0^2 \tag{1}$$

where $k_0 = 2\pi/\lambda$ is the vacuum wavevector, n_1 the refractive index of the fiber glass, and β the longitudinal component of the wavevector. In the region surrounding the waveguiding core with refractive index n_2 the transverse wavevector,

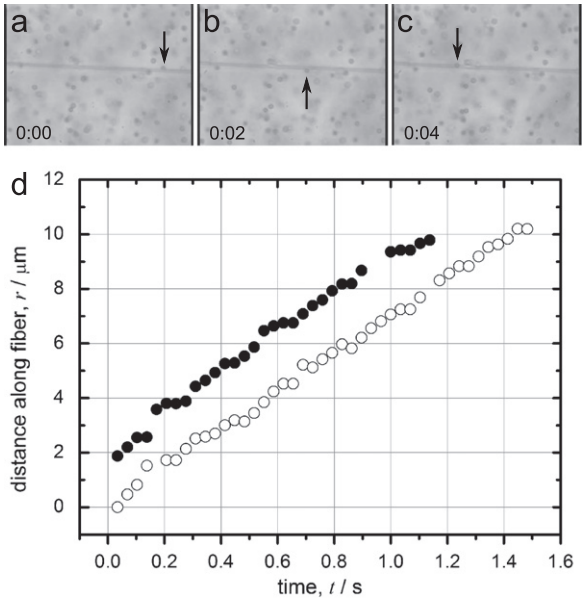

Fig. 2. Particle tracking video microscopy of propelled microparticles. (a)–(c) Sequence of frames taken from a movie at intervals of 2 s showing optical binding and propulsion of a 2 μm diameter polystyrene sphere (indicated by the black arrow) in the evanescent field surrounding a tapered optical fiber; (d) reconstruction of the trajectories of two particles (represented by the different symbols) moving at uniform velocity along the fiber.

q satisfies

$$q^2 = \beta^2 - n_2^2 k_0^2 \tag{2}$$

and is imaginary, implying a rapidly decaying evanescent field. As an example we show in Fig. 3 the field distributions for a silica glass tapered fiber with parameters approximately those of the experiment in Section 2.2. The fiber is surrounded by water and has diameter $a = 1.0$ μm, and is supporting a quasi-linearly ($x-$) polarized HE_{11} mode. The normalized frequency of this tapered fiber, $V = ka\sqrt{n_1^2 - n_2^2} = 2.048$, is below the cut-off frequency for single-mode operation, $V_C = 2.405$, thus the HE_{11} modes are the only modes supported by this waveguide. As shown in [25] the strong confinement of the initially (quasi-) linearly polarized HE_{11} fiber mode in the taper leads to significant components of electric field in the orthogonal directions.

For the HE_{11} mode initially polarized in the x-direction the dominant component remains the x-polarized field, shown in Fig. 3(a) but the amplitudes of the electric fields in the y- and z-directions become significant for large refractive index differences between the silica fiber and its surroundings (large fiber numerical aperture), shown in Fig. 3(b) and (c). Similar cross-polarized components are also observed in the case of high numerical aperture focusing, e.g. by a microscope objective lens [26]. Furthermore, the conditions for continuity of electric field components normal and tangential to the boundary lead to an enhancement of the evanescent electric

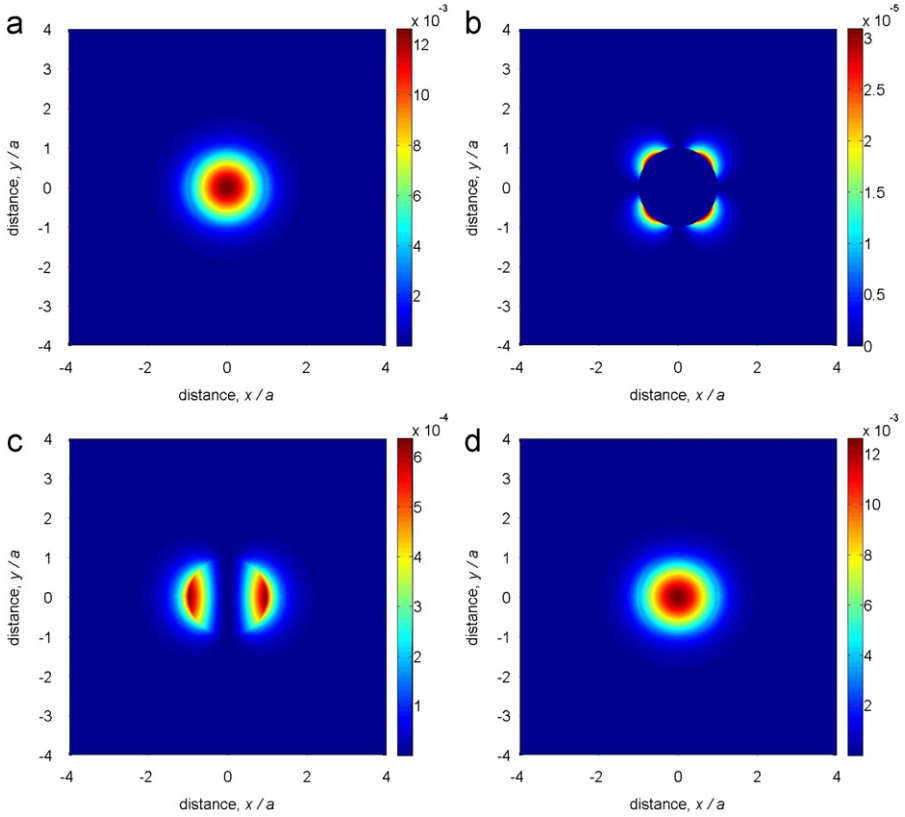

Fig. 3. Intensity of the electric field in a tapered silica optical fiber, radius 500 nm, optical wavelength $\lambda_0 = 1064$ nm for the quasi-linearly polarized HE_{11} mode; (a) field in the x- (dominant polarization) direction; (b) field in the y- (orthogonal transverse) direction; (c) field in the z- (propagation) direction; (d) total field.

field along the x-axis, resulting in a net field distribution with pronounced lobes along $\pm x$, shown in Fig. 3(d). The evanescent field of this mode penetrates a significant distance into the surroundings. For these exemplar parameters we calculate a penetration depth $\Lambda = |q|^{-1} = 0.39\ \mu\text{m}$, and approximately 26% of the mode power carried in the evanescent field.

3.2. Interaction with metallic nanoparticles

Metallic nanoparticles have unique useful optical properties due to the plasmon resonance in their scattering spectrum [27]. The enhancement of optical forces exerted on the nanoparticle that arises when the laser wavelength is tuned close to the plasmon resonance can be utilized to achieve stable optical trapping in single-beam optical tweezers [28,29] which might otherwise be difficult due to the volume scaling of optical gradient forces for such small particles [30], and recently good agreement between experimental measurement and theoretical calculation of trapping forces has been demonstrated for both single metallic spheres [31,32] and aggregates of nanoparticles [33]. Hybridization of metallic nanoparticles with objects such as whispering-gallery resonators or quantum dots and the resultant coupling between the plasmon and the narrow resonances has even been suggested as a novel method for achieving laser-cooling of these mesoscopic systems [34].

Evanescent wave manipulation of gold nanoparticles has been demonstrated using the field of a channel waveguide fabricated by an ion-exchange technique [35], and enhancement of optical forces using the surface plasmon of a thin gold film has also been applied to manipulation of both polystyrene [36] and gold particles [37].

Here we consider the manipulation of silver nanoparticles in the evanescent field around the tapered fiber. The motivation for using silver nanoparticles is that in addition to their potentially useful technological applications [38], the optical properties lend themselves to an additional degree of control over the optical forces. The relatively narrow plasmon resonance lineshape of silver when compared to, for example, gold leads to a region on the short-wavelength side of the resonance where the real part of the polarizability of the nanoparticle can be negative [39], and so the direction of the optical gradient force is reversed, which may be exploited to induce particle repulsion from a surface [42]. This situation is analogous to that used in the 'gravito-optical surface trap' for ultra-cold atoms [43].

First we consider the interaction between a nanoparticle and the evanescent field of a tapered optical fiber supporting a HE_{11} mode of a wavelength tuned to the long-wavelength side of the plasmon resonance (red detuning). The optical properties of the silver nanoparticles are calculated using a Lorentz–Drude model [44] using the fitting parameters tabulated in [45] which produce a good fit to the experimental data of [46,47] in the range 0.125–6 eV ($\lambda = 200-1000$ nm).

An example of the calculated optical properties is shown in Fig. 4 for a spherical silver nanoparticle of radius 20 nm. Part (a) of Fig. 4 shows the real part of the complex polarizibility, $\text{Re}\{\alpha(\lambda)\}$ calculated in the range $\lambda_0 = 350-700$ nm. Of particular interest for the present

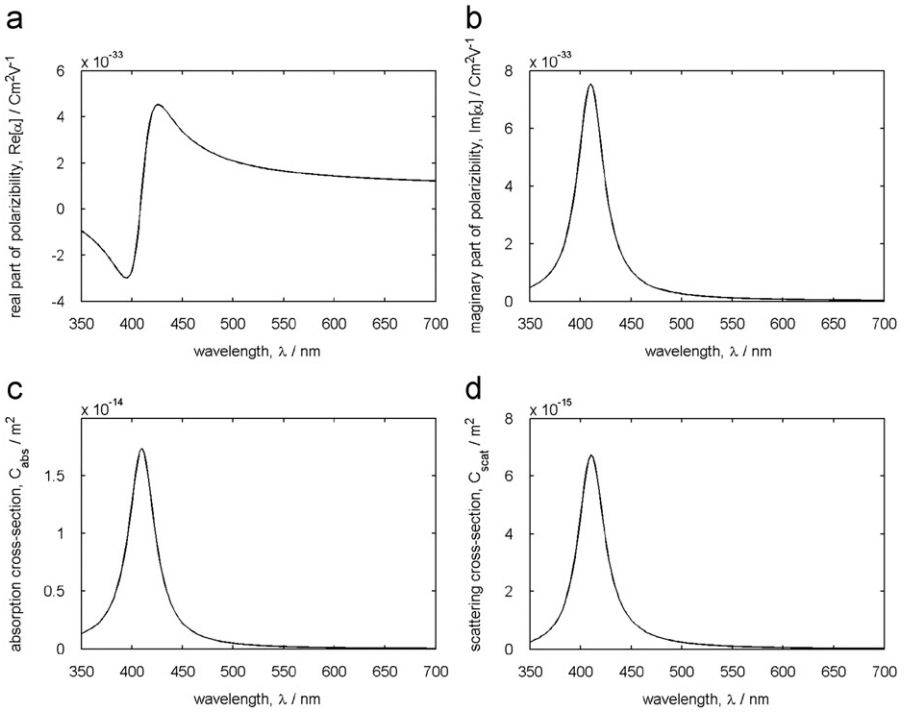

Fig. 4. Optical properties of a 40 nm diameter spherical silver nanoparticle as a function of wavelength calculated from the Lorentz–Drude model; (a) real part of the polarizibility, $\text{Re}\{\alpha\}$; (b) imaginary part of the polarizibility, $\text{Im}\{\alpha\}$; (c) absorption cross-section, C_{abs}; (d) scattering cross-section, C_{scat}.

work is the change in sign of $\mathrm{Re}\{\alpha\}$ in the region of the plasmon resonance with $\mathrm{Re}\{\alpha\}<0$ for blue detunings and $\mathrm{Re}\{\alpha\}>0$ for red detunings. Part (b) shows the imaginary part of the polarizibility, $\mathrm{Im}\{\alpha(\lambda)\}$ with a clear resonance feature around $\lambda_p = 408$ nm. This resonance leads to the peaks in the absorption, C_{abs}, and scattering, C_{scat}, cross-sections shown in Fig. 4(c) and (d), respectively, which are related to the polarizibility as

$$C_{\mathrm{abs}} = \frac{k}{\epsilon_0}\mathrm{Im}\{\alpha(\lambda)\} \tag{3}$$

$$C_{\mathrm{scat}} = \frac{k^4}{6\pi\epsilon_0^2}\left|\alpha(\lambda)\right|^2 \tag{4}$$

3.3. Monochromatic trapping

We treat small (Rayleigh) particles as dipoles and account for depolarization effects at small but finite volume with the correction to the dipolar response of [48]. The interaction between a point dipolar particle and an optical beam is usually separated into two parts. Firstly a force arising from a spatial gradient in the dipole potential energy,

$$\mathbf{F}_{\mathrm{grad}} = -\frac{1}{4}\mathrm{Re}\{\alpha\}\nabla|E|^2 \tag{5}$$

that acts in the direction of a gradient of intensity in the beam, and secondly an optical scattering force,

$$\mathbf{F}_{\mathrm{scat}} = \frac{C_{\mathrm{ext}}}{c}\langle\mathbf{S}\rangle \tag{6}$$

where $C_{\mathrm{ext}} = C_{\mathrm{abs}} + C_{\mathrm{scat}}$ is the total extinction cross-section that acts in the direction of the time-averaged Poynting vector, $\mathbf{S} = \frac{1}{2}\mathrm{Re}\{\mathbf{E}\times\mathbf{H}^*\}$. Recently a third component of optical force arising from the non-uniform distribution of the spin density of an optical field has been identified [49,50],

$$\mathbf{F}_{\mathrm{spin}} = cC_{\mathrm{ext}}(\nabla\times\langle\mathbf{L}_S\rangle) \tag{7}$$

where

$$\langle\mathbf{L}_S\rangle = \frac{\epsilon_0}{4\omega i}(\mathbf{E}\times\mathbf{E}^*) \tag{8}$$

is the time-averaged spin density. This contribution to the optical force (sometimes called the 'spin curl force') is the most significant for strongly localized fields such as in the focal volume of a high numerical aperture objective lens [51] and may be expected to play a role in the highly non-paraxial fields of a sub-micron tapered optical fiber. Consistent with previous work analyzing a similar system for trapping of nanoparticles [40], in calculating the optical forces we neglect the effects of multiple scattering between the nanoparticle and the tapered fiber. This approximation can be made provided the nanoparticle is not too close to the substrate (fiber), and the contrast in dielectric constant between the substrate and suspending medium is relatively low [41].

Let us take as an example the 40 nm diameter spherical silver nanoparticle considered above, and examine the interaction with the evanescent field of a tapered optical fiber with radius $a = 0.15$ μm. We calculate the electric field distribution of an x-polarized HE_{11} mode as above, and calculate the dipole potential energy for a number of different wavelengths taking into account also the dispersion of the silica glass of the optical fiber using tabulated Sellmeier coefficients [52]. The dipole interaction energies are then shown in Fig. 5(a)–(d), plotted in units of $k_{\mathrm{B}}T$ (k_{B} Boltzmann's constant) at temperature $T = 293$ K, and normalized per unit power contained in the mode (i.e. the sum of the power carried in the fiber core and the power in the evanescent field).

The plasmon wavelength for the silver nanoparticle is found to be $\lambda_{\mathrm{p}} \approx 408$ nm. Fig. 5(a) shows the interaction energy for a laser wavelength tuned slightly to the long-wavelength side of the plasmon (red detuning), with $\lambda = 425$ nm. As expected there is a minimum of potential energy adjacent to the fiber, which is deepest along the predominant direction of polarization. For a laser wavelength detuned to the short wavelength side of the plasmon (blue detuning), with $\lambda = 395$ nm, the sign of the dipole potential is reversed, shown in Fig. 5(b), and the dipole potential repels the nanoparticle from the fiber. Fig. 5(c) and (d) demonstrates the effect of further detuning to the red side of the plasmon resonance as the potential well becomes both shallower and broader as the wavelength becomes longer and the evanescent field penetrates further into the surrounding medium. In Fig. 5(c), $\lambda = 633$ nm and the penetration depth $\Lambda_{633} = 1.64$ μm, and in Fig. 5(d), $\lambda = 2\lambda_{\mathrm{p}} = 816.7$ nm and the penetration depth $\Lambda_{816.7} = 12.4$ μm.

For unidirectional mode propagation in the tapered fiber, in addition to the gradient force that traps particles against the fiber, there is also a radiation pressure (scattering force and 'spin curl' force) directed parallel to the fiber that propels the particles along it, as seen in Fig. 2. For plasmonic nanoparticles the magnitude of the propelling force is maximum when the laser is tuned to the plasmon resonance, where we find for the cross-sections $C_{\mathrm{abs}} = 1.72\times10^{-14}$ m^2 and $C_{\mathrm{scat}} = 6.58\times10^{-15}$ m^2, and a maximum propelling force adjacent to the fiber of $F_z = 507$ pN W^{-1}, decreasing to $F_z = 84$ pN W^{-1} at a distance from the fiber equal to the fiber radius (these forces are also normalized per unit power in the mode). At this distance approximately 90% of the force arises from the radiation pressure, and the remaining 10% from the curl of the spin density. The resulting propagation speed of the nanoparticle along the fiber is estimated from the Stokes drag on a sphere corrected for the presence of a cylindrical boundary [53] to be $v_z = 224$ mm s^{-1} W^{-1}.

Detuning to the red of the plasmon resonance such that gradient force trapping is achievable, we find at e.g. $\lambda = 425$ nm the cross-sections are reduced to $C_{\mathrm{abs}} = 8.87\times10^{-15}$ m^2 and $C_{\mathrm{scat}} = 4.34\times10^{-15}$ m^2, and the propelling force at a distance $d=a$ from the fiber reduced to $F_z = 50$ pN W^{-1}. In this situation we estimate the nanoparticle velocity along the fiber to be $v_z = 134$ mm s^{-1} W^{-1}. These forces can be balanced by using counter-propagating modes with parallel polarizations [9] in the fiber, which will also modulate the intensity (and hence the optical dipole potential) along the length of the fiber providing an additional degree of localization [40].

Using a circularly polarized HE_{11} mode changes all components of the forces acting on the nanoparticle. Firstly the optical dipole potential becomes symmetric

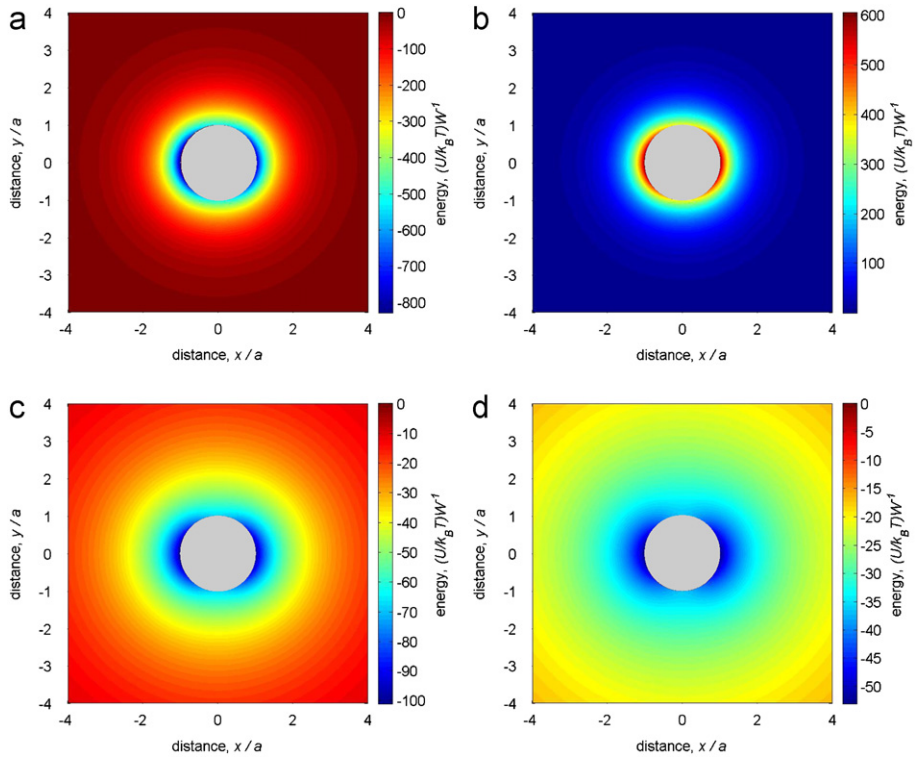

Fig. 5. Electric dipole interaction energy between 40 nm diameter silver nanoparticle (plasmon wavelength, $\lambda_p = 413.35$ nm) and the evanescent field surrounding a 150 nm radius tapered glass fiber as a function of wavelength; (a) $\lambda = 408.35$ nm; (b) $\lambda = 395$ nm; (c) $\lambda = 633$ nm; (d) $\lambda \approx 2 \times \lambda_p = 816.7$ nm. The gray circle in the middle of each figure represents the glass fiber.

around the fiber due to the rapidly rotating polarization direction. Secondly the Poynting vector acquires a component that acts in the azimuthal direction arising from the longitudinal component of the electric field, which contains an azimuthal phase variation similar to that which occurs in a free-space Laguerre–Gaussian laser mode. Thirdly the spin curl force also acquires an azimuthal component. For a high numerical aperture fiber there is a significant field component in the longitudinal direction, and for small diameter tapers a significant fraction of the optical power resides in the evanescent field outside the fiber. The net effect of these features is that a particle in the evanescent field may experience strong non-conservative forces arising from the optical scattering and spin curl contributions. Fig. 6(a) and (b) shows the distribution of the intensity of the transverse and longitudinal electric field components, respectively, for a circularly polarized HE_{11} mode of a tapered optical fiber with the same diameter as above and at the plasmon wavelength of the 40 nm silver nanoparticle, $\lambda = \lambda_p$. As a result of the circular polarization there is now an azimuthal symmetry to the time-averaged electric field distribution. In parts (c) and (d) of Fig. 6 we show the spatial distributions of the longitudinal, S_z, and azimuthal, S_ϕ, components of the Poynting vector, respectively. The presence of non-zero azimuthal components of Poynting vector and curl of the spin density gives rise to an additional component of the force transverse to the axis of the fiber, and it may therefore expected that a circularly polarized HE_{11} mode will drive a nanoparticle in a helical trajectory along and around the taper. Fig. 7(a) and (b) shows the resulting electric dipole interaction energy at wavelengths detuned to the red and blue (respectively) of the plasmon resonance for the same 40 nm diameter silver nanoparticle in the vicinity of $a = 150$ nm fiber. In this case the azimuthally directed component of the non-conservative (scattering + spin curl) force, F_ϕ can be significant compared to F_z, and we find for an exemplar case of red detuning from the plasmon resonance, $\lambda = 425$ nm an axial component of force (normalized) of $F_z = 47$ pN W^{-1} at a distance $d = a$ from the fiber, and an azimuthal component of $F_\phi = 7$ pN W^{-1}. In the absence of an azimuthally modulated gradient force we therefore expect the nanoparticles to be attracted to the fiber and pushed along it following a helical trajectory in a manner previously calculated for ultra-cold atoms [54]. From this we estimate (normalized) components of velocity of the nanoparticle of $v_z = 126$ mm s^{-1} W^{-1} in the axial direction and $v_\phi = 17$ mm s^{-1} W^{-1} in the azimuthal direction.

3.4. Bichromatic trapping

The ability to tune the interaction, and in particular produce either attractive or repulsive forces depending on the detuning from resonance naturally leads to the possibility of using two wavelengths simultaneously to obtain an extra degree of control over the optical trapping. The formation of a two-color or bichromatic trap for

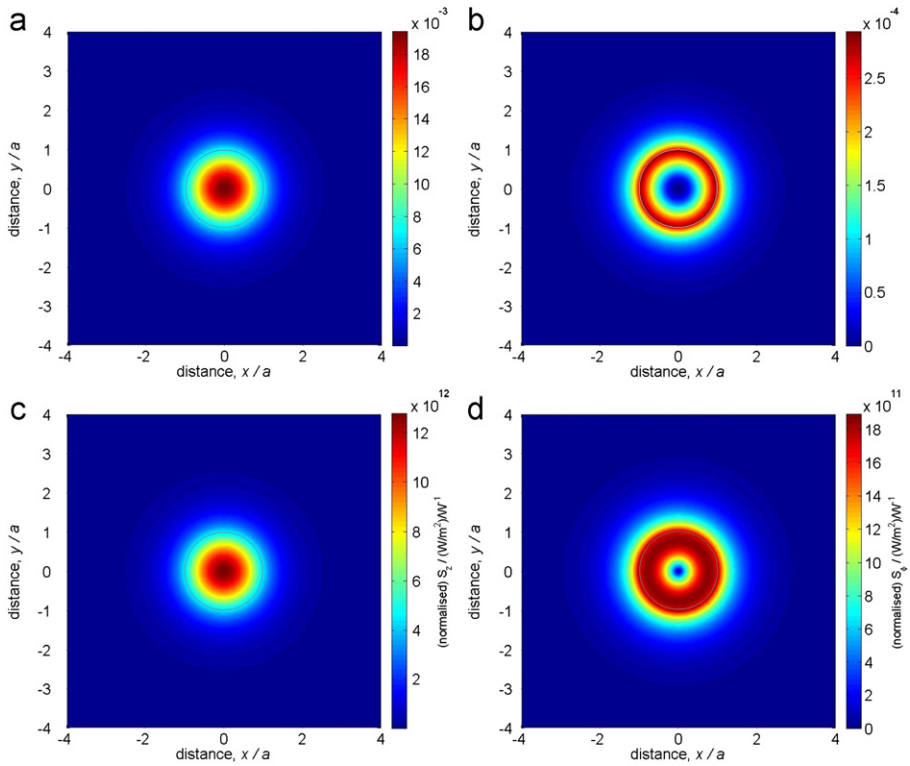

Fig. 6. Intensity of the electric field distribution and magnitude of Poynting vector for a circularly polarized HE_{11} mode in a tapered optical fiber, radius $a = 150$ nm for a wavelength $\lambda = \lambda_p = 408$ nm; (a) transverse electric field; (b) longitudinal electric field; (c) longitudinal component of the Poynting vector, S_z; (d) azimuthally directed component of the Poynting vector, S_ϕ. The gray circle in the middle of each figure represents the diameter of the glass fiber.

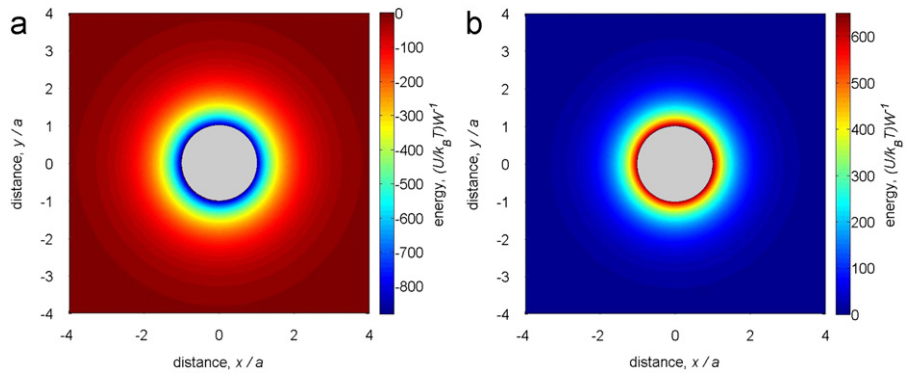

Fig. 7. Interaction potentials for a circularly polarized HE_{11} mode in a tapered optical fiber, radius $a = 150$ nm with a 40 nm diameter silver nanoparticle. $\lambda_p = 408$ nm; (a) wavelength $\lambda = 425$ nm $> \lambda_p$; (b) wavelength $\lambda = 425$ nm $> \lambda_p$. The gray circle in the middle of each figure represents the diameter of the glass fiber.

ultra-cold atoms in the evanescent field of a tapered fiber was considered in [55], and similar detuning-dependence of forces in an evanescent field have been considered for metallic nanoparticles and also for microparticles exhibiting whispering gallery modes [56]. As can be seen in Fig. 5 the penetration depths, Λ, of the evanescent fields depend on the optical wavelength, and due to the width of the plasmon resonance (some tens of nanometers for our silver nanoparticles) for two wavelengths detuned to the red and blue of λ_p these can be significantly different. A plasmonic nanoparticle exposed to these evanescent fields may therefore experience competing gradient forces: one from the red-detuned beam that draws it toward the fiber, and one from the blue-detuned beam that provides a potential barrier preventing it from reaching the fiber surface.

Fig. 8 shows some examples of the bichromatic potential experienced by the 40 nm silver nanoparticle around a fiber carrying two counter-propagating (parallel) linearly polarized HE_{11} modes with different wavelengths.

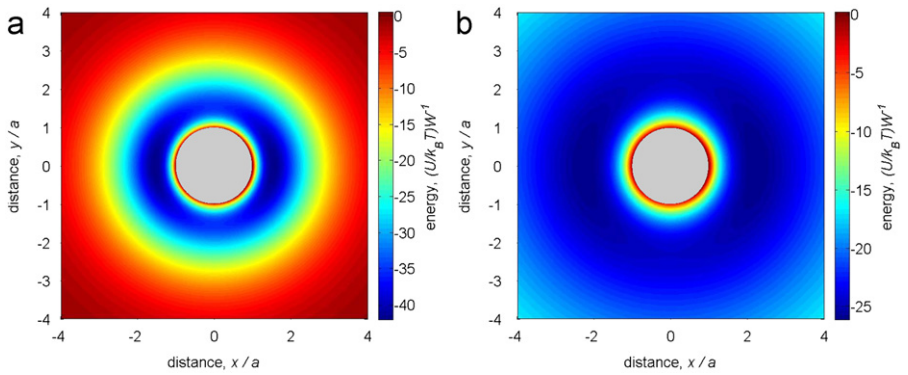

Fig. 8. Interaction potentials for two wavelengths of linearly polarized HE_{11} modes in a tapered optical fiber, radius $a = 150$ nm with a 40 nm diameter silver nanoparticle. $\lambda_p = 408$ nm; (a) wavelengths $\lambda_R = 425$ nm and $\lambda_B = 395$ nm; (b) wavelengths $\lambda_R = 816.7$ nm and $\lambda_B = 405$ nm. The gray circle in the middle of each figure represents the diameter of the glass fiber.

The powers of the two modes are chosen such that the net potential energy is zero adjacent to the fiber. In part (a) the longer wavelength, $\lambda_R = 425$ nm, and the shorter wavelength is $\lambda_B = 397$ nm. For this combination the intensity of the blue-detuned mode is 1.37 times that of the red-detuned mode. Two potential minima can be seen a small distance from the fiber along the $\pm x$-axis. At this equilibrium trapping position the radiation pressures from the two beams are unequal. Due to the width of the plasmon resonance (some tens of nanometers) the typical difference in frequency between the red- and blue-detuned laser modes used to realize a bichromatic trap is sufficiently large that the effects of beating of the two frequencies may be neglected and the forces arising from the two modes simply added [57]. The net scattering force (radiation pressure + spin curl forces) on the nanoparticle arising from this configuration is found to be 113 pN W^{-1} at the minimum of the dipole potential, which would drive the nanoparticle at an estimated speed of $v_z = 460$ mm s^{-1}. For a different combination of wavelengths the fraction of optical power in the evanescent field and the decay lengths are different. By way of example part (b) of Fig. 8 uses wavelengths $\lambda_R = 816.7$ nm $= 2\lambda_p$ and $\lambda_B = 407$ nm (very close to resonance). For these parameters the blue-detuned mode has an intensity 0.19 times that of the red-detuned mode. The potential minima can be seen to be broader, shallower, and displaced further from the fiber. At this equilibrium position the net radiation pressure from the counter-propagating beams is only 180 pN W^{-1} and a velocity of $v_z = 178$ mm s^{-1}.

When considering the utility of this technique for particle sorting and separation it is instructive to compare with a number of other methods that have previously appeared in the literature. A 'near-field' sorting technique was demonstrated for micron-sized particles in [58], where the evanescent field was created using a TIR objective lens. In this geometry the extent of the interaction region is limited to the size of the laser beam spot (given as 13.4 μm), whereas a tapered fiber can potentially produce a useful evanescent field for many tens of microns along the tapered region. Similarly, the large separation between particle collection regions at opposite ends of the taper may be advantageous when compared to the scheme of [59] where the relative displacements for particles of different sizes are comparatively small. The method of [60] uses a dynamic (translating or flashing) optical lattice for very effective separation of particles according to size or composition. By contrast the tapered fiber method proposed for sorting particles would not require active modulation of parameters during an experiment as the optical forces depend on the detuning from the plasmon resonance, and are thus strongly dependent on nanoparticle size and composition. The initial choice of laser wavelengths therefore controls the selectivity of the technique.

4. Conclusions

In conclusion, we have experimentally demonstrated that microscopic particles can be attracted to and propelled along sub-micron scale glass fibers by the evanescent field of a laser beam. We have made calculations of the optical gradient and scattering forces of the evanescent field for metallic (silver) nanoparticles and shown how control of the fiber mode polarization and wavelength can be used to control motion of nanoparticles along the fiber. We anticipate that the sensitivity of the interaction to nanoparticle plasmonic properties and fiber mode distribution could potentially be a useful tool for selectively trapping, sorting and trafficking micro- and nanoparticles drawn from a polydisperse distribution.

Acknowledgements

This work is supported by the Royal Society, EPSRC (UK) and NanoScience Europe. S.E.S. thanks the UCL Graduate School for a scholarship, R.P. and E.K. acknowledge research bursaries from the Nuffield Foundation. We thank M. Rashid for useful discussions.

References

[1] Ashkin A, Dziedzic JM, Bjorkholm JE, Chu S. Observation of a single-beam gradient force optical trap for dielectric particles. Opt Lett 1986;11:288–90.

[2] Ashkin A, Dziedzic JM. Optical trapping and manipulation of viruses and bacteria. Science 1987;235:1517–20.
[3] Burnham DR, McGloin D. Holographic optical trapping of aerosol droplets. Opt Exp 2006;14:4175–81.
[4] Jones PH, Maragó OM, Stride EPJ. Parametrization of trapping forces on microbubbles in scanning optical tweezers. J Opt A Pure Appl Opt 2007;9:S278–83.
[5] Irrera A, Artoni P, Saija R, Gucciardi PG, Iatì MA, Borghese F, et al. Size-scaling in optical trapping of silicon nanowires. Nano Lett 2011;11:4879–84.
[6] Maragó OM, Gucciardi PG, Bonaccorso F, Calogero G, Scardaci V, Rozhin A, et al. Optical trapping of carbon nanotubes. Physica E 2008;40:2347–51.
[7] Maragó OM, Bonaccorso F, Saija R, Privitera G, Gucciardi PG, Iatì MA, Calogero G, Jones PH, Borghese F, Denti P, Nicolosi V, Ferrari AC. Brownian motion of graphene. ACS Nano 2010;4:7515–23.
[8] Kawata S, Sugiura T. Movement of micrometer-sized particles in the evanescent field of a laser beam. Opt Lett 1992;17:772–4.
[9] Mellor CD, Bain CD. Array formation in evanescent waves. ChemPhysChem 2006;7:329–32.
[10] Lekner J. Force on a scatterer in counter-propagating coherent beams. J Opt A Pure Appl Opt 2005;7:238–48.
[11] Mellor CD, Fennerty TA, Bain CD. Polarization effects in optically bound particle arrays. Opt Exp 2006;14:10079–88.
[12] Summers MD, Dear RD, Taylor JM, Ritchie GAD. Directed assembly of optically bound matter. Opt Exp 2012;20:1001–12.
[13] van Leeuwen NJ, Moore LJ, Partridge WD, Peverall R, Ritchie GAD, Summers MD. Near-field optical trapping with an actively locked cavity. J Opt 2011;13:044007-1–5.
[14] Bures J, Ghosh R. Power density of the evanescent field in the vicinity of a tapered fiber. J Opt Soc Am A 1999;16:1992–6.
[15] Sagué G, Vetsch E, Alt W, Meschede D, Rauschenbeutel A. Cold-atom physics using ultrathin optical fibers: light-induced dipole forces and surface interactions. Phys Rev Lett 2007;99:163602-1–5.
[16] Morrissey MJ, Deasy K, Wu Y, Chakrabarti S, Nic Chormaic S. Tapered optical fibers as tools for probing magneto-optical trap characteristics. Rev Sci Instrum 2009;80:053102-1–5.
[17] Brambilla G, Senthil Murugan G, Wilkinson JS, Richardson DJ. Optical manipulation of microspheres along a subwavelength optical wire. Opt Lett 2007;32:3041–3.
[18] Yang AHJ, Moore SD, Schmidt BS, Klug M, Lipson M, Erickson D. Optical manipulation of nanoparticles and biomolecules in sub-wavelength slot waveguides. Nature 2009;457:71–5.
[19] Ahluwalia BS, Subramanian AZ, Hellesø OG, Perney NMB, Sessions NP, Wilkinson JS. Fabrication of submicrometer high refractive index Tantalum Pentoxide waveguides for optical propulsion of microparticles. IEEE Photon Technol Lett 2009;21:1408–10.
[20] Ahluwalia BS, Løvhaugen P, Hellesø OG. Waveguide trapping of hollow glass spheres. Opt Lett 2011;36:3347–9.
[21] Brambilla G, Finazzi V, Richardson DJ. Ultra-low-loss optical fiber nanotapers. Opt Exp 2004;12:2258–63.
[22] Birks TA, Li YW. The shape of fiber tapers. J Lightwave Technol 1992;10:432–8.
[23] Crocker JC, Grier DG. Methods of digital video microscopy for colloidal studies. J Coll Interf Sci 1996;179:298–310.
[24] Yariv A. Optical electronics. 3rd ed.New York: CBS College Publishing; 1985.
[25] Kien FL, Liang JQ, Hakuta K, Balykin VI. Field intensity distributions and polarization orientations in a vacuum-clad subwavelength-diameter optical fiber. Opt Commun 2004;242:445–55.
[26] Rashid M, Maragó OM, Jones PH. Focusing of high-order cylindrical vector beams. J Opt A Pure Appl Opt 2008;11:065204-1–7.
[27] Klar T, Perner M, Grosse S, von Plessen G, Spirkl W, Feldmann J. Surface-plasmon resonances in single metallic nanoparticles. Phys Rev Lett 1998;80:4249–52.
[28] Hansen PM, Bhatia VK, Harrit N, Oddershede L. Expanding the optical trapping range of gold nanoparticles. Nano Lett 2005;5:1937–42.
[29] Bosanac L, Aabo T, Bendix PM, Oddershede LB. Efficient optical trapping and visualization of silver nanoparticles. Nano Lett 2008;8:1486–91.
[30] Molloy JE, Padgett MJ. Lights, action: optical tweezers. Contemp Phys 2002;43:241–58.
[31] Saiji R, Denti P, Borghese F, Maragò OM, Iatí MA. Optical trapping calculations for metal nanoparticles. Comparison with experimental data for Au and Ag spheres. Opt Exp 2009;12:10231–41.
[32] Hajizadeh F, Reihani SNS. Optimized optical trapping of gold nanoparticles. Opt Exp 2010;18:551–9.
[33] Messina E, Cavallaro E, Cacciola A, Iatí MA, Gucciardi PG, Borghese F, et al. Plasmon-enhanced optical trapping of gold nanoaggregates with selected optical properties. ACS Nano 2011;5:905–13.
[34] Ridolfo A, Saija R, Savasta S, Jones PH, Iatì MA, Maragó OM. Fano-Doppler laser cooling of hybrid nanostructures. ACS Nano 2011;9:7354–61.
[35] Ng LN, Zervas MN, Wilkinson JS, Luff BJ. Manipulation of colloidal gold nanoparticles in the evanescent field of a channel waveguide. Appl Phys Lett 2000;76:1993–5.
[36] Volpe G, Quidant R, Badenes G, Petrov D. Surface plasmon radiation forces. Phys Rev Lett 2006;96:238101-1–4.
[37] Wang K, Schonbrun E, Crozier KB. Propulsion of gold nanoparticles with surface plasmon polaritons: evidence of enhanced optical force from near-field coupling between gold particle and gold film. Nano Lett 2009;9:2623–9.
[38] Liau SY, Read DC, Pugh WJ, Furr JR, Russell AD. Analysis of the toxic mode of action of silver nanoparticles using stress-specific bioluminescent bacteria. Lett Appl Microbiol 1997;25:279–83.
[39] Albaledjo S, Marqués MI, Sáenz JJ. Light control of silver nanoparticle's diffusion. Opt Exp 2011;19:11471–8.
[40] Zhao L, Li Y, Qi J, Xu J, Sun Q. Quasi 3-dimensional optical trapping by two counter-propagating beams in nano-fiber. Opt Exp 2010;18:5724–9.
[41] Román-Velázquez CE, Noguez C, Barrera RG. Substrate effects on the optical properties of spheroidal nanoparticles. Phys Rev B 2000;61:10427–36.
[42] Chaumet PC, Nieto-Vesperinas M. Electromagnetic force on a metallic particle in the presence of a dielectric surface. Phys Rev B 2000;62:11185–91.
[43] Ovchinnikov YuB, Manek I, Grimm R. Surface trap for Cs atoms based on evanescent-wave cooling. Phys Rev Lett 1997;79:2225–8.
[44] Ung B, Sheng Y. Interference of surface waves in a metallic nanoslit. Opt Exp 2007;15:1182–90.
[45] Rakic AD, Djurišic AB, Elazar JM, Majewski ML. Optical properties of metallic films for vertical-cavity optoelectronic devices. Appl Opt 1998;37:5271–83.
[46] Dold B, Mecke R. Optische Eigenschaften von Edelmetallen, Übergangsmetallen und deren Legierungen im Infrarot (1. Teil). Optik 1965;22:435–46.
[47] Winsemius P, Langkeek HP, vanKampen FF. Structure dependence of the optical properties of Cu, Ag and Au. Physica 1975;79B:529–46.
[48] Meier M, Wokaun A. Enhanced fields on large metal particles: dynamic depolarization. Opt Lett 1983;8:581–3.
[49] Wong V, Ratner MA. Gradient and nongradient contributions to plasmon-enhanced optical forces on silver nanoparticles. Phys Rev B 2006;73:075416-1–6.
[50] Albaladejo S, Marqués MI, Laroche M, Sáenz JJ. Scattering force from the curl of the spin of the angular momentum of a light field. Phys Rev Lett 2009;102:113602-1–4.
[51] Iglesias I, Sáenz JJ. Scattering forces in the focal volume of high numerical aperture microscope objectives. Opt Commun 2011:2430–6.
[52] Malitson IH. Interspecimen comparison of the refractive index of fused silica. J Opt Soc Am 1965;55:1205–9.
[53] Cox RG. The motion of suspended particle almost in contact. Int J Multiphase Flow 1974;1:343–71.
[54] Kien FL, Balykin VI, Hakuta K. Light-induced force and torque on an atom outside a nanofiber. Phys Rev A 2006;74:033412-1–8.
[55] Kien FL, Balykin VI, Hakuta K. Atom trap and waveguide using a two-color evanescent light field around a subwavelength-diameter optical fiber. Phys Rev A 2004;70:063403-1–9.
[56] Xiao JJ, Zheng HH, Sun YX, Yao Y. Bipolar optical forces on dielectric and metallic nanoparticles by evanescent wave. Opt Lett 2010;35:962–4.
[57] Ploschner M, Čižmar T, Mazilu M, Di Falco A, Dholakia K. Bidirectional optical sorting of gold nanoparticles. Nano Lett 2012;12:1923–7.
[58] Marchington RF, Mazilu M, Kuriakose S, Garcés-Chávez V, Reece PJ, Krauss T, et al. Optical deflection and sorting of microparticles in a near-field optical geometry. Opt Exp 2008;16:3712–26.
[59] Grzegorczyk TT, Kemp BA, Kong JA. Passive guiding and sorting of small particles with optical binding forces. Opt Lett 2006;31:3378–80.
[60] Smith RL, Spalding GC, Dholakia K, MacDonald MP. Colloidal sorting in dynamic optical lattices. J Opt A Pure Appl Opt 2007;9:S134–8.